ELSEVIER

Mathematical Biosciences 176 (2002) 145–159

Mathematical Biosciences

www.elsevier.com/locate/mbs

Temporal classification of *Drosophila* segmentation gene expression patterns by the multi-valued neural recognition method

Igor Aizenberg [a], Ekaterina Myasnikova [b,*], Maria Samsonova [b], John Reinitz [c]

[a] *Neural Networks Technologies (NNT) Ltd., 155 Bialik st., Ramat-Gan 52523, Israel*
[b] *Institute of High Performance Computing and Data Bases, 118 Fontanka emb., St. Petersburg 198005, Russia*
[c] *Department of Applied Mathematics and Statistics, The University at Stony Brook, Stony Brook, NY 11794-3600, USA*

Received 17 May 2001; received in revised form 29 June 2001; accepted 20 November 2001

Abstract

In order to reconstruct the establishment of the body pattern over time in *Drosophila* embryos, we have developed automated methods for detecting the age of an embryo on the basis of knowledge about its gene expression patterns. In this paper we perform temporal classification of confocal images of expression patterns of genes controlling segmentation by means of a neural network based on multi-valued neurons (MVN). MVN are artificial neural processing elements with complex-valued weights and high functionality, which proved to be efficient for solving the image recognition problems. The results obtained by this method confirm its efficiency for image recognition and indicate that the method can detect characteristic features of expression patterns which mark their development over time.

Keywords: Gene expression; *Drosophila*; Functional genomics; Classification; Neural networks; Multi-valued neurons

1. Introduction

Studies of gene expression are of fundamental importance to the field of functional genomics. Functional genomics itself will ultimately involve the application of genomics to all areas of

* Corresponding author.
E-mail addresses: igora@netvision.net.il (I. Aizenberg), myasnikova@fn.csa.ru (E. Myasnikova), samson@fn.csa.ru (M. Samsonova), reinitz@ams.sunysb.edu (J. Reinitz).

0025-5564/02/$ - see front matter
PII: S0025-5564(01)00104-3

biological function, including animal development. In the development of an embryo, fields of initially uniform cells become determined to follow diverse developmental pathways as a result of differential gene expression. Over time, spatially uniform or low resolution patterns of gene expression transform into precise expression patterns of high spatial resolution, often to the level of a single cell. This process is not yet susceptible to study by DNA microarrays, because this technology requires the homogenization of tissue samples before assay, thus destroying information about the spatial distribution of gene products. Nevertheless, the precise characterization of spatially regulated gene expression patterns will become central to functional genomics as these technological barriers are overcome. Such characterization will raise novel computational questions which can be dealt with now in a suitable biological system.

The biological system which we consider is the segment determination system of the fruit fly *Drosophila melanogaster*, which sets up a chemical blueprint for the animal's body segments. The genetics of this system has been characterized, and it has been shown that the segmentation network is made up of a reasonably small network of identified genes [2–4,11,13,22,26]. We believe that the full characterization of this system at the level of functional genomics requires the construction of fully dynamical model [7,8,18–20]. In order to generate a sufficiently accurate model, we must quantitatively characterize the expression patterns at cellular spatial resolution and a temporal resolution comparable to the time required for a visible change in expression, which is about five or ten minutes. How to achieve this temporal resolution is the subject of this paper.

The problem arises from the following experimental situation. Data are acquired by confocal scanning microscopy from fixed embryos, each of which is stained by fluorescence methods to show the pattern of expression of three protein gene products [6]. Thus, the temporal dynamics must be reconstructed from many samples, each at a different stage of development. A fundamental step in such a reconstruction is to determine the developmental age of each embryo. As it is not experimentally possible to obtain fully synchronized embryos, it is desirable to obtain the age directly from the expression pattern itself. Previously this determination was made by experienced human observers. This paper describes a way to make the determination automatically. The patterns in question exist when the embryo is a hollow, roughly ellipsoidal shell of nuclei. These patterns can be viewed as a collection of 'domains', each of which is a region of expression containing one maximum. Repeating domains are referred to as 'stripes', and some genes such as *even-skipped* (*eve*), which is under consideration in the present study, have very dynamic patterns in which a broad initial domain later resolves into stripes (see Figs. 1 and 2).

Our goal is to develop precise and automated methods to assign a developmental age to an embryo on the basis of knowledge about its gene expression patterns. The methods for temporal staging will be developed in two steps. The first is to automatically classify embryos into one of the manually determined time classes, and the second is to automatically assign a specific developmental age. In this paper we address only the first of these issues. The most important corollary of a successful classification is the ability to detect the characteristic features of expression patterns which mark their development over time. The dynamics of gene expression could then be described by the dynamics of a small number of parameters which describe these features as the expression domains change over time.

The solution to the temporal classification problem presented here is based on neural nets constructed from multi-valued neurons (MVN) which operate on complex-valued data [17]. The

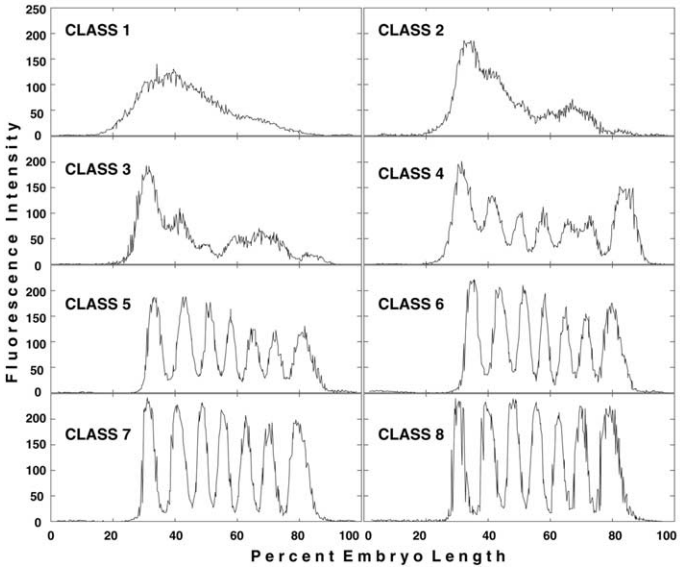

Fig. 1. Representative 1D *eve* expression patterns belonging to each of the eight temporal classes, as labeled. The *x*-axis is labeled in percent egg length from anterior to posterior; the *y*-axis shows fluorescence levels in 8 bit units.

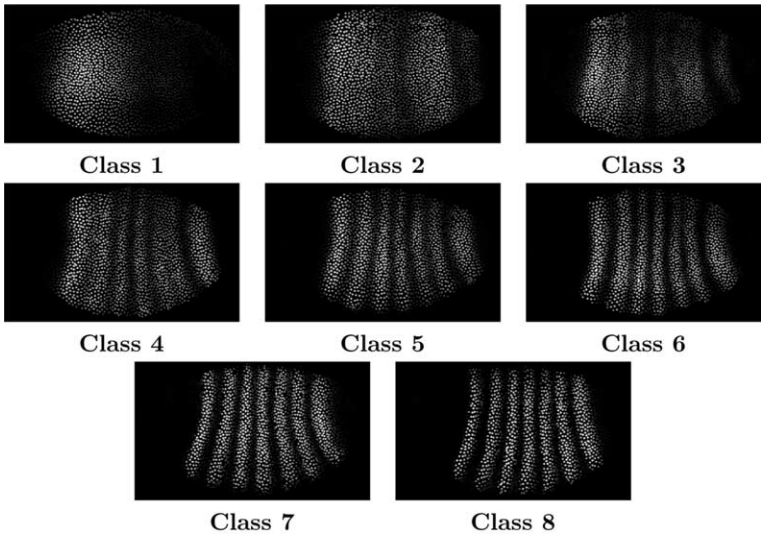

Fig. 2. Representative images of segmented and rescaled *eve* expression patterns belonging to the eight temporal classes. Each nucleus is represented by a single pixel whose intensity is proportional to the average fluorescence level at that nucleus.

ability of classical artificial neural networks to classify objects and processes by means of learning algorithms makes their application to pattern recognition both promising and attractive [27]. In particular, different kinds of neural networks have been successfully used in solving an image

recognition problem [12]. It is always difficult to formalize the image description so that it can be adapted for learning. One solution to this challenge is a transformation of the image presentation to the frequency domain. This choice makes a natural fit with complex valued MVN.

2. System and methods

2.1. The dataset

In our experiments gene expression was measured using fluorescence tagged antibodies as described [6]. For each embryo a 1024×1024 pixel confocal image with eight bits of fluorescence data in each of three channels was obtained. To acquire the data in terms of nuclear location an image segmentation procedure was applied [5,10]. The segmentation procedure transforms the image into an ascii table containing a series of data records, one for each nucleus. Each nucleus is characterized by a unique identification number, the x and y coordinates of its centroid, and the average fluorescence levels of three proteins. The embryo is oriented so that the x-axis corresponds to the anterior–posterior (A–P) axis of the embryo and the y-axis to the dorsal–ventral (D–V) axis. In the segmented data files, x and y coordinates are expressed as percent of the maximum size of the embryo in the x and y directions. Finally, the processed images are rescaled to remove non-specific background signal.

In this work we describe the application of classification methodology to a group of 736 embryos from Oregon-R flies stained for 13 segmentation genes. Each embryo was stained for the *eve* segmentation gene and two others that vary among the dataset. All of these embryos belong to cleavage cycle 14A [29]. This cycle is about an hour long and is characterized by a rapid transition of the *eve* gene expression patterns, which culminates in the formation of seven stripes.

2.2. Preliminary temporal classification

The 736 embryos were divided into eight temporal classes [9]. The goal of temporal classification is to obtain groups of embryos which are indistinguishable with respect to the temporal development of expression patterns. Each embryo is allocated to one of the temporal classes on the basis of thorough and extensive visual inspection of gene expression patterns, particularly that of *eve*, which is highly dynamic. The classification was performed by placing all of the embryos into a partially ordered set, which was then divided into eight discrete classes. This number was chosen to capture definitive changes in the pattern. Thus while some temporal ordering is possible within a class, its members have very similar expression patterns for each gene. The 736 embryos from cycle 14A were selected for scanning without regard for age, and the eight classes are approximately equally populated, so we expect our dataset to be uniformly distributed in time. Since cycle 14A is about 50 min long [29], each class represents a little over 6 min.

The evolution of the expression patterns of *eve* during cleavage cycle 14A is shown in Fig. 1. Time classes 1–4 do not have seven well-defined *eve* stripes and the number and location of stripes changes rapidly. The remaining groups (classes 5–8) do have seven well-defined stripes. After all the stripes are clearly visible their intensities increase in the posterior portion of the embryo. By the end of cycle 14A, all *eve* stripes have reached maximum and equal intensity and maximum sharpness.

Time classes 1–4 are grouped according to the number of individual *eve* domains which have formed. The remaining groups (classes 5–8) all have seven well-defined *eve* stripes and were classified by features of the overall *eve* pattern along with the patterns of other genes.

2.3. Methods

The neural network described in this paper was implemented using a software simulator developed in IINPRISE (BORLAND) DELPHI 5.0 for Windows 95 and higher. The filter used for the extraction of image details was implemented on the same platform. These programs have been tested and used on Pentium-III PCs running Windows NT 4.0 or Windows 98.

3. Preliminary results: one-dimensional classification by the discriminant function analysis

The essential step for automated pattern classification in time is to characterize the patterns in terms of some observable parameters, and then use these parameters to read off the time. Expression of segmentation genes is largely a function of position along the A–P axis of the embryo body, and so can be well represented in one dimension. The preliminary time classification of expression patterns was performed for data extracted from the central 10% of y values on the midline of an embryo, which runs parallel to the x-axis. The y values of these data are then ignored, and the patterns, demonstrating the variation of gene expression along the x-axis, are presented as graphs. The stripes and interstripes then have the form of peaks and valleys respectively (see Fig. 1).

As it is clear from the figure, it is natural to use extrema of expression domains as a set of variables for classification, but the noise on the peaks makes it rather difficult to find the extrema locations directly from the raw data. There exist many methods based on different principles for extracting the features from a one-dimensional (1D) signal of this type. We have employed the quadratic spline approximation as well as the wavelet transform to extract extremal features of the pattern [9,10,21]. The classification of 1D images was performed by means of discriminant function analysis [28]. Discriminant analysis is mainly used to determine which variables discriminate between two or more naturally occurring groups. Another major purpose to which discriminant analysis is applied is the issue of predictive classification of objects. For each group in our sample, we can determine the location of the point that represents the means for all variables in the multivariate space defined by the variables in the model. These points are called group centroids. For each object we can then compute the Mahalanobis distances [28] (of the respective object) from each of the group centroids. The Mahalanobis metric is defined by

$$D = (\mu_C - \mu_O)\mathbf{V}^{-1}(\mu_C - \mu_O), \tag{1}$$

where μ_C and μ_O are the vectors of features of the group centroid and object respectively, and $\mathbf{V}$ is the covariance matrix of the group. Again, we would classify the object as belonging to the group to which it is closest, that is, where the Mahalanobis distance is smallest. Discriminant analysis will automatically compute the classification functions, which can be used to determine to which

Table 1
Recognition results for 1D data obtained by discriminant analysis

Class #	4	5	6	7	8
Training set	33	36	30	30	36
Number of images to be recognized	43	77	86	62	40
Recognized	36 (83.7%)	38 (49.4%)	51 (59.3%)	38 (61.3%)	27 (67.5%)
Misclassified	7	39	35	24	13

group each object most likely belongs. There are as many classification functions as there are groups. Each function allows us to compute classification scores for each object for each group, by applying the formula:

$$S_i = c_i + w_{i1}y_1 + w_{i2}y_2 + \cdots + w_{im}y_m. \tag{2}$$

In this formula, the subscript i denotes the respective group; the subscripts $1, 2, \ldots, m$ denote the variables; c_i is a constant for the ith group, w_{ij} is the weight for the jth variable in the computation of the classification score for the ith group; y_j is the observed value of jth variable for the respective expression pattern. S_i is the resultant classification score. Now we classify the pattern as belonging to the group for which it has the highest classification score. We estimate the discriminant functions that best discriminate between groups, based on some training data set, and then use them when predicting the other cases that were not used for the estimation of the discriminant function. Assigning embryos of a continuous range of ages to discrete classes requires drawing somewhat arbitrary borders between temporal classes. Thus an embryo whose age places it close to a border may look somewhat atypical for the class to which it was assigned. To characterize a time class more definitely we use a set of representative patterns chosen to be from the central part of the temporal class as a training set.

This method is appropriate for expression patterns at intermediate and late development stages when a full set of domains has formed. The recognition results are shown in Table 1. The class 4 images are best recognized (the attribution is 83.7%). Other embryo images are allocated to their classes with an accuracy of 49.4–67.5%. Thus the classification method is not very reliable (maximal attribution error is 50.6%). The reason for the high accuracy of recognition of embryos belonging to temporal class 4 may be the strong difference of the *eve* expression pattern at this age in comparison with other temporal classes.

As we have concluded from our previous study it makes no sense to try to improve the classification results by applying other methods to the set of fixed features of 1D signal. To raise the quality of classification, we dropped the restriction to 1D data and used more powerful classifiers. Though expression of segmentation genes is largely a 1D function of position on the x-axis, features of two-dimensional (2D) images will supply more information to the classifier. Moreover, our choice of the characteristic features was based on a fixed set of features. We need to apply a more advanced classification method which makes an automated choice of the features responsible for the distribution of objects over the classes. In the next section we show that MVN-based neural networks achieve better temporal classification when applied to our whole dataset, including the very early embryos which were not considered in our previous classification.

4. Multi-valued neuron and MVN-based neural networks for image recognition

4.1. Multi-valued neuron

The concept of the MVN was introduced by one of us [24], and has been comprehensively presented in terms of theory and applications elsewhere [17]. Here we briefly review key mathematical properties of MVN networks and their learning algorithms.

An MVN performs a mapping between n inputs and a single output which may take on k values. The mapping is described by a function of n variables characterized by $n+1$ complex-valued weights $w_0, w_1, \ldots, w_n$, so that

$$f(x_1, \ldots, x_n) = P(w_0 + w_1 x_1 + \cdots + w_n x_n). \tag{3}$$

Here $x_1, \ldots, x_n$ are the neuron's inputs or in other words the variables on which the function depends. All of the x_i as well as $f(x_1, \ldots, x_n)$ are one of the kth complex roots of unity, and each of k possible logical values are represented by one such root, denoted as $\varepsilon^j = \exp(\mathrm{i}2\pi j/k)$, with $j \in \{0, k-1\}$, $\mathrm{i}^2 = -1$. P is the activation function of a neuron:

$$P(z) = \exp(\mathrm{i}2\pi j/k) \quad \text{if } 2\pi j/k \leqslant \arg(z) < 2\pi(j+1)/k, \tag{4}$$

where $j = 0, 1, \ldots, k-1$ are the values of the k-valued logic, $z = w_0 + w_1 x_1 + \cdots + w_n x_n$ is the weighted sum, and $\arg(z)$ is the argument θ of the complex number $z = R\exp(\mathrm{i}\theta)$. So, if z belongs to the jth sector of the complex plane, the output of a neuron described by Eq. (4) is equal to ε^j (Fig. 3).

MVN have some wonderful properties which make them much more powerful than traditional artificial neurons. The representation (3) and (4) makes possible an implementation of the input/output mappings described by arbitrary partially defined multiple-valued functions. We do not need to pay attention in this case to the complexity of the partial complicated mapping. Any mapping may be implemented using a single neuron. This makes it possible to develop neural networks adapted for solving complicated applied problems.

Another important property of MVN is the simplicity of their learning algorithms. Theoretical aspects of the learning, which are based on motion within the unit circle, have been discussed in [17]. Considering MVN learning as a generalization of perceptron learning [27], we obtain the

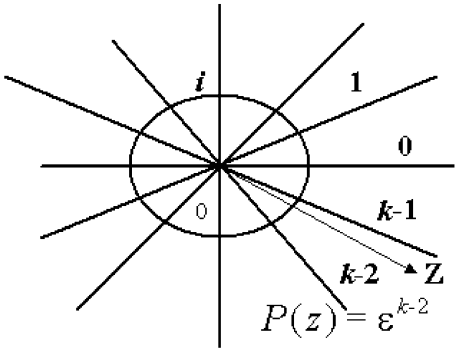

Fig. 3. Illustration of the MVN activation function.

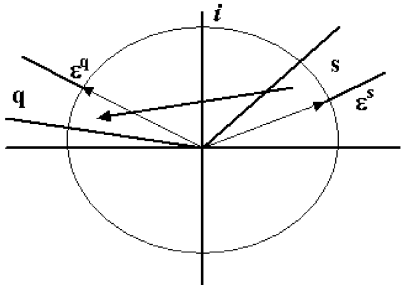

Fig. 4. MVN learning.

following. If a perceptron output is incorrect for an element of the learning set (1 instead of -1, or -1 instead of 1) then the weights have to be corrected according to some rule to ensure an inversion of the weighted sum sign. Therefore, it is necessary to move the weighted sum to the opposite subdomain (respectively, from 'positive' to 'negative', or from 'negative' to 'positive').

For the MVN, which performs a mapping described by a k-valued function we have exactly k domains. Geometrically they are sectors on the complex plane (Fig. 3). If the desired output of the MVN on some element from the learning set is equal to ε^q then the weighted sum has to be placed into the qth sector. But if the actual output is equal to ε^s the weighted sum is assigned to sector number s (see Fig. 4). The learning rule must correct the weights so as to move the weighted sum from sector s to sector q. We use here a previously proposed correction rule for MVN learning [17]

$$W_{m+1} = W_m + \frac{C_m}{(n+1)}(\varepsilon^q - \varepsilon^s)\overline{X}, \tag{5}$$

where W_m and W_{m+1} are the current and next weighting vectors, $\overline{X}$ is the complex conjugate of the vector of the neuron's input signals, ε is a primitive kth root of unity chosen from (4), C_m is a scale coefficient, q is the desired sector on the complex plane, s is the sector into which the actual value of the weighted sum has fallen, and n is the number of inputs to the neuron. Since the learning rule (5) is linear, it is easy to implement and converges quickly. Elsewhere [17] it has been shown that given any partially defined multiple-valued function $f(x_1, \ldots, x_n)$, it is always possible to find a k such that f can be implemented in an MVN so that Eq. (3) will hold. But once such an f is implemented in an MVN, it can be proved that the learning rule (5) converges [17]. It is this set of properties that make the MVN approach so powerful.

4.2. MVN-based neural network for pattern recognition

Let us consider N classes of objects, which are presented by images of $n \times m$ pixels. The problem is formulated in the following way: we have to create a recognition system based on a neural network which affords successful classification of the objects by fast learning on the minimal number of representatives from all the classes.

MVN-based neural networks and the methods of its organization have been proposed in the form of such a system [16], and further developed elsewhere [15,17]. The frequency domain

representation of the data is very important for this model. All 2D images are replaced by their Fourier spectra. Moreover, taking into account that a spectral phase contains more information about an object presented by a signal than the amplitude [1], only the spectral phase is used for an object representation. (The spectral amplitude contains more information about the signal behavior, presence of noise or blur (if any), etc.) It has been observed [23] that objects belonging to the same class must have similar coefficients corresponding to low frequencies.

For different classes of discrete signals the sets of quarter to half low frequency spectral coefficients are very close for the signals belonging to the same class from the standpoint of learning and analysis on the neural network [23]. This observation is true for different orthogonal transformations. To classify an object in terms of neural networks we have to train a neural network on a learning set containing the spectral phase of representatives of the classes. Then the weights obtained in the learning will be used for the classification of unknown objects.

Representation of the recognized objects by phases of the Fourier spectral coefficients is ideal for an MVN-based neural network. Since the inputs and outputs of an MVN are complex numbers and moreover roots of unity, it is natural to use phases as the inputs. The logical structure of the MVN suggests how to make use of phase while neglecting amplitude: rather than normalize, we put the inputs into correspondence with the value of k in (4) by applying the same transformation. So a phase of θ is transformed according to

$$P(\theta) = \exp(\mathrm{i}2\pi j/k) \quad \text{if } 2\pi j/k \leqslant \theta < 2\pi(j+1)/k. \tag{6}$$

An MVN-based single layer neural network, which contains the same number of neurons as the number of classes to be classified (Fig. 5) has been considered [15,17]. Each neuron has to recognize a pattern belonging only to its class and to reject any pattern from any other class.

This system has been successfully tested on an example of face recognition [15]. In practice, the best results have been obtained when the first $l = k/2$ sectors on the complex plane represent the l classes of faces to be recognized. The other $k/2$ sectors correspond to rejected patterns (Fig. 6).

Extraction of the phases from Fourier spectral coefficients is organized according to frequency ordering. We start from the lowest ones and then we proceed according to the so-called 'zig-zag' rule (Fig. 7).

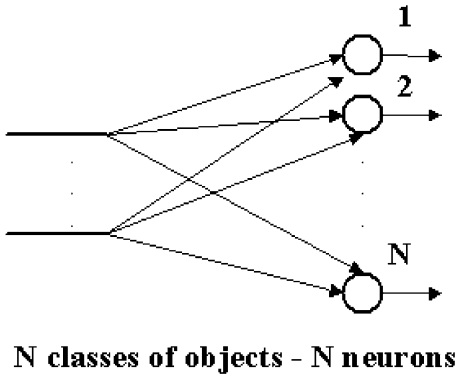

Fig. 5. MVN-based neural network for image recognition.

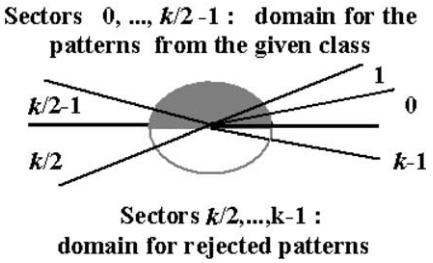

Fig. 6. Reservation of the domains for the face recognition example.

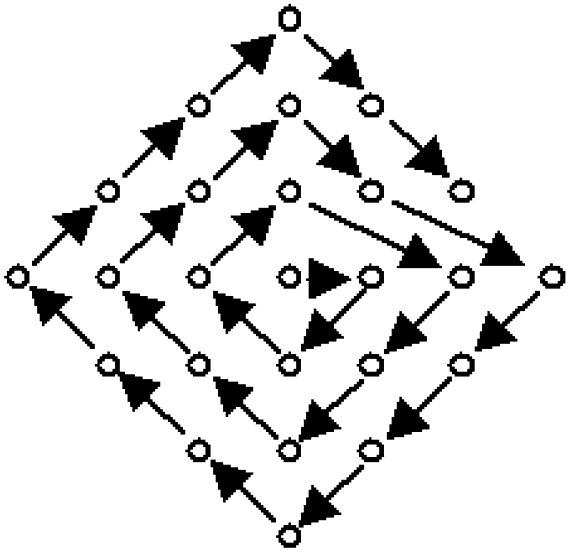

Fig. 7. Extraction of the phases according to the 'zig-zag' rule. We are going by diagonals starting from the 0th spectral coefficient. Diagonals corresponding to the same 2D frequency are at an equal distance from the 0th spectral coefficient.

5. Recognition and classification: simulation results

To solve the classification problem we used the MVN-based neural network described above. In order to use 2D gene expression information without the complications introduced by the cytological fine structure in a confocally scanned micrograph, we 'reconstituted' images from files of segmented expression data by creating 256×256 pixel images in which each identified nucleus is represented by setting the pixel which contains its coordinates to a value equal to the average fluorescence level for that nucleus. Examples of these images are shown in Fig. 2. For the purpose of better visualization, these images are plotted with rectangular pixels whose aspect ratio is chosen to be the same as the aspect ratio of a nucleus; these plots look similar to micrographs of stained embryos.

Since the expression patterns from neighboring classes are often similar to each other, the architecture of the network has been modified in the following dichotomous way. A three-layered network was used. Two neurons of the first layer classify patterns into those belonging to classes 1–4

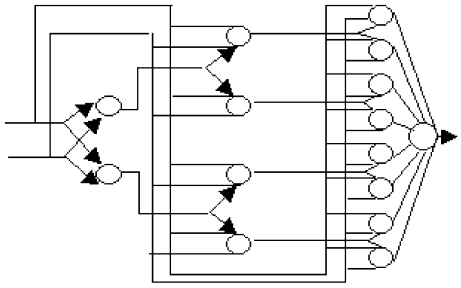

Fig. 8. The dichotomous neural network architecture used for temporal classification.

or 5–8. Four neurons of the second layer classify a pattern into one of the classes 1–2, 3–4, 5–6 and 7–8. Finally, eight neurons of the third layer classify a pattern into a particular class (Fig. 8), and the single neuron of the output layer analyzes the results coming from the neurons of the third layer.

To create the representative learning sets for all the neurons, we used images that have been a priori correctly classified as representative for the particular class. This classification is based on the objective biological view described in Section 3. Since it is natural to teach the neural network using maximally distinguished data, the definitively representative images have been included in the learning set (from 28 to 35 images per class) and the other images were used for testing.

The choice of k was made empirically. Large values of k allow high precision phase information to travel through the net. We found that for the problem considered here, the best performance was obtained with neurons of at least $k = 2048$, and the work reported here set k to that value. We used inputs taken from the Fourier phase coefficients corresponding to frequencies from 1 to 6. Since there are 84 discrete Fourier spectral coefficients corresponding to these frequencies, each neuron will have 84 inputs. All the neurons were taught using a learning algorithm based on rule (5). Learning converged quickly (10–15 s per neuron using the software implementation on Intel Pentium-III-700 processor). The results of testing are given in Table 2 for the final third layer. The percent of recognized images is fairly high, with a maximal attribution error of 31.5% (for comparison, 50.6% by discriminant analysis Table 1). However there still remain a certain number of unrecognized and misclassified images. Here we need to specify the terminology used in the table. Misclassification is a false attribution of an image to the certain class, while it is a priori known as belonging to a different class. Unrecognized images are those which are rejected by the neural network to be classified as belonging to any class. Each neuron from the network is designed for the classification of the patterns from one class and for the rejection of all other patterns.

Table 2
Final classification results from the third layer of neurons

Class #	1	2	3	4	5	6	7	8
Number of images	75	43	68	55	78	89	67	53
Recognized	61 (81.3%)	30 (69.7%)	49 (72%)	45 (81.8%)	59 (75.6%)	61 (68.5%)	46 (68.7%)	38 (71.7%)
Unrecognized	3	1	1	1	1	3	1	1
Misclassified	11	12	18	9	18	25	20	14

We should note here that it is due to the dichotomous architecture of the neural network that 'misclassification' lies in an erroneous attribution of an image almost without exception to a neighbor temporal class. It is in not more than 1% of cases that an image may be attributed to a more distinct class. Such a structure of the network (Fig. 8) was chosen to minimize a percent of misclassified images and it provides much better results as compared to the single-level architecture which was used previously for the image recognition on the MVN-based neural network [15].

It is clear from Fig. 2 that the images are of low contrast and many of important details remain invisible. Moreover, the small level of brightness jumps between important details of the images negatively affects the informational capacity of the Fourier representation of the image. Phases of the image spectrum corresponding to neighboring classes are sometimes very close to each other. As a result, the number of misclassified images still remains relatively high, especially for the neurons of the third layer. To fix this problem it is natural to use a filter, which can amplify high spatial frequencies while preserving at the same time low and medium spatial frequencies. High frequency amplification makes it possible to enhance a contrast of the smallest objects against a residual image background.

We used the following spatial domain filter for preprocessing:

$$\hat{B}_{ij} = (G_1 + G_2)B_{ij} - G_2 B_{\mathrm{m}} + c, \tag{7}$$

where B_{m} is the local mean value in a 3×3 window surrounding the pixel B_{ij}; B_{ij} and $\hat{B}_{ij}$ are the signal values in ijth pixel before and after processing, respectively; G_1 defines the correction of the low spatial frequencies, G_2 defines the correction of the high spatial frequencies, c is the mean value of the background after processing. This filter is called the high frequency correction filter and it has been considered, for example, in [14]. Note that if $G_1 = 1$, the filter (7) coincides with the 'unsharp masking' filter in different applications [30].

The significant improvement of image quality after applying the filter (7) is shown in Fig. 9, which shows the same images which are presented in Fig. 2 processed with the filter (7).

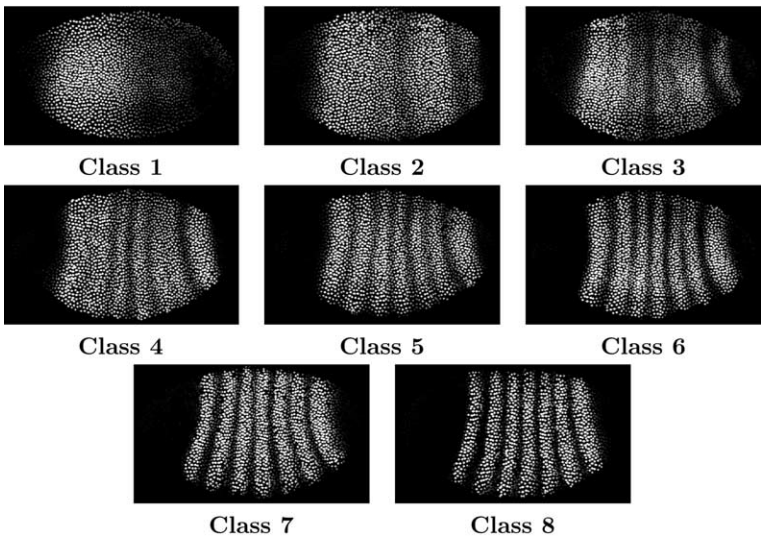

Fig. 9. Images presented in Fig. 2 subjected to preprocessing with filter (7).

Table 3
Final classification results from the third layer of neurons using preprocessed images

Class #	1	2	3	4	5	6	7	8
Number of images	75	43	68	55	78	89	67	53
Recognized	65 (86.6%)	31 (72.1%)	51 (75.0%)	50 (90.9%)	61 (78.2%)	65 (75.0%)	47 (70.2%)	42 (79.3%)
Unrecognized	3	1	1	0	1	0	1	1
Misclassified	7	11	16	5	16	24	19	10

The filter was applied to all the images from all the classes. Then the recognition technique presented above was tested again using the images obtained after filtering. The learning and testing sets were composed of the same images as before. The learning process required approximately the same time, while the classification was improved. Table 3 presents the final classification results for layer 3 of the neural network. Comparing these results to the corresponding results presented in Table 2, one can see that the recognition is increased by 2–9% and therefore the proposed preprocessing technique proved to be very important for the classification improvement.

6. Conclusions

In this paper we have demonstrated substantial progress in solving the temporal classification problem for early *Drosophila* embryos. Early work [10] cannot be directly compared with the results here because the learning and generalization task was posed differently, but the 1D discriminant analysis presented in this paper is essentially the method used earlier but with Mahalanobis distance employed instead of Euclidean distance. Discriminant analysis performed comparatively poorly: with the exception of class 4, accuracy was in the range of 49–67%. Moreover, the smaller number and greater variability of extrema in early embryos render this method unsuitable for classes 1 through 4.

To improve classification we applied the MVN-based neural network to the recognition of 2D data. This produced a substantial improvement. All temporal classes were now susceptible to classification, with accuracy ranging from 69% to 82%. With preprocessing, this rose to an accuracy range of 70–91%. This level of accuracy is very promising, but not yet at a sufficiently high level to use this method for high throughput temporal classification. Nevertheless, there is reason to believe that the situation is more favorable than it appears, as we now explain.

We do not know, as yet, to what extent the observed misclassifications reflect inaccuracies of the recognition method as opposed to the preliminary classification by human observers. Moreover, subdivision of the dataset into a certain number of classes is somewhat arbitrary and therefore assigning the borders of these classes is also quite arbitrary. The placement of borders means that two embryos in different classes can have patterns that are more similar that each has to 'distant' members of its own class.

We are conducting studies now that may resolve this issue. Certain cytological events can be observed both in vivo and in fixed tissue, and standardization of in vivo events against a physical

clock gives us an absolute timing standard for fixed tissue. For example, it is possible to measure membrane invagination in vivo and construct a reasonably precise standard curve giving membrane invagination as a function of clock time [25]. We think it likely that this information will enable us to perfect an accurate temporal classifier suitable for routine usage.

In particular, Fourier decomposition is a natural methodological choice for the classification. The analysis of the Fourier coefficients used for classification will be very important for further work. Then the most significant coefficients will form a set of features which describe the dynamics of gene expression in time. For example, it will be important to analyze the significance of each spectral coefficient for the classification. The estimation of informational capacity of the Fourier spectral phases used for classification may be implemented using analysis of the weights obtained as the learning results. Large weights correspond to the most important features, and the small weights correspond to less significant features. Fourier analysis is also a natural choice biologically. A skilled human observer placing embryos in temporal order is essentially ordering them based on increasing spatial resolution of the expression patterns, and this has a natural concomitant in the Fourier components.

Acknowledgements

This work is supported by NIH grants 1 RO3 TW01147-01 and RO1 RR07801-08, NATO Collaborative Linkage Grant LST 975850, GAP awards RBO-685 and RBO-895, and the Ministry of Science and Technologies of the Russian Federation. The work is partially supported by the company Neural Networks Technologies (NNT-Israel) Ltd.

References

[1] A.V. Oppenheim, S.J. Lim, The importance of phase in signals, Proc. IEEE 69 (1981) 529.
[2] C. Nusslein-Volhard, E. Wieschaus, Mutations affecting segment number and polarity in *Drosophila*, Nature 287 (1980) 795.
[3] C. Nusslein-Volhard, E. Wieschaus, H. Kluding, Mutations affecting the pattern of the larval cuticle in *Drosophila melanogaster* I. Zygotic loci on the second chromosome, Roux's Arch. Develop. Biol. 193 (1984) 267.
[4] C. Nusslein-Volhard, H. Kluding, G. Jurgens, Genes affecting the segmental subdivision of the *Drosophila* embryo, Cold Spring Harbor Symp. Quant. Biol. 50 (1985) 145.
[5] D. Kosman, J. Reinitz, D.H. Sharp, Automated assay of gene expression at cellular resolution, in: R. Altman, K. Dunker, L. Hunter, T. Klein (Eds.), Proceedings of the 1998 Pacific Symposium on Biocomputing, Singapore, World Scientific Press, 1997, p. 6. http://www.smi.stanford.edu/projects/helix/psb98/kosman.pdf.
[6] D. Kosman, S. Small, J. Reinitz, Rapid preparation of a panel of polyclonal antibodies to *Drosophila* segmentation proteins, Develop. Genes, Evol. 208 (1998) 290.
[7] D.H. Sharp, J. Reinitz, Prediction of mutant expression patterns using gene circuits, BioSystems 47 (1998) 79.
[8] E. Mjolsness, D.H. Sharp, J. Reinitz, A connectionist model of development, J. Theor. Biol. 152 (1991) 429.
[9] E. Myasnikova, A. Samsonova, K. Kozlov, M. Samsonova, J. Reinitz, Registration of the expression patterns of *Drosophila* segmentation genes by two independent methods, Bioinformatics 17 (1) (2001) 3.
[10] E. Myasnikova, D. Kosman, J. Reinitz, M. Samsonova, Spatio-temporal registration of the expression patterns of *Drosophila* segmentation genes, in: T. Lengauer et al. (Ed.), Proceedings of the 7th International Conference on Intelligent Systems for Molecular Biology, AAAI, Menlo Park, CA, 1999, p. 195.

[11] E. Wieschaus, C. Nusslein-Volhard, G. Jurgens, Mutations affecting the pattern of the larval cuticle in *Drosophila melanogaster* III. Zygotic loci on the X-chromosome and fourth chromosome, Roux's Arch. Develop. Biol. 193 (1984) 296.
[12] C.T. Leondes (Ed.), Image Processing and Pattern Recognition, Academic Press, San Diego, CA, 1997.
[13] G. Jurgens, E. Wieschaus, C. Nusslein-Volhard, H. Kluding, Mutations affecting the pattern of the larval cuticle in *Drosophila melanogaster* II. Zygotic loci on the third chromosome, Roux's Arch. Develop. Biol. 193 (1984) 283.
[14] I.N. Aizenberg, Processing of noisy and small-detailed gray-scale images using cellular neural networks, J. Electron. Imag. 6 (3) (1997) 272.
[15] I.N. Aizenberg, Neural networks based on multi-valued and universal binary neurons: theory, application to image processing and recognition, Lecture Notes in Computer Science, vol. 1625, Springer, Berlin, 1999, p. 306.
[16] I.N. Aizenberg, N.N. Aizenberg, Application of the neural networks based on multi-valued neurons in image processing and recognition, SPIE Proc. 3307 (1998) 88.
[17] I.N. Aizenberg, N.N. Aizenberg, J. Vandewalle, Multi-valued and Universal Binary Neurons: Theory, Learning, Application, Kluwer Academic, Boston, MA, 2000.
[18] J. Reinitz, D. Kosman, C.E. Vanario-Alonso, D. Sharp, Stripe forming architecture of the gap gene system, Develop. Genet. 23 (1998) 11.
[19] J. Reinitz, D.H. Sharp, Mechanism of formation of eve stripes, Mech. Develop. 49 (1995) 133.
[20] J. Reinitz, E. Mjolsness, D.H. Sharp, Cooperative control of positional information in *Drosophila* by *bicoid* and maternal *hunchback*, J. Exp. Zool. 271 (1995) 47.
[21] K. Kozlov, E. Myasnikova, M. Samsonova, J. Reinitz, D. Kosman, Method for spatial registration of the expression patterns of *Drosophila* segmentation genes using wavelets, Comput. Technol. 5 (2000) 112.
[22] M. Akam, The molecular basis for metameric pattern in the *Drosophila* embryo, Development 101 (1987) 1.
[23] N. Ahmed, K.R. Rao, Orthogonal Transforms for Digital Signal Processing, Springer, Berlin, 1975.
[24] N. Aizenberg, I. Aizenberg, Cnn based on multi-valued neuron as a model of associative memory for gray-scale images, in: A. Sanfeliu et al. (Ed.), Proceedings of the 2nd IEEE Int. Workshop on Cellular Neural Networks and their Applications, Munich, Germany, 2–14 October 1992, p. 36.
[25] P.T. Merrill, D. Sweeton, E. Wieschaus, Requirements for autosomal gene activity during precellular stages of *Drosophila melanogaster*, Development 104 (1988) 495.
[26] P.W. Ingham, N.E. Baker, A. Martinez-Arias, Regulation of segment polarity genes in the *Drosophila* blastoderm by *fushi tarazu* and *even skipped*, Nature 331 (1988) 73.
[27] S. Haykin, Neural Networks, A Comprehensive Foundation, Macmillan College, New York, 1994.
[28] S.J. Press, Applied Multivariate Analysis, Holt, Rinehart & Winston, New York, 1972.
[29] V.A. Foe, B.M. Alberts, Studies of nuclear and cytoplasmic behaviour during the five mitotic cycles that precede gastrulation in *Drosophila* embryogenesis, J. Cell Sci. 61 (1983) 31.
[30] W.K. Pratt, Digital Image Processing, John Wiley, New York, 1992.